

Adaptive Sampling to Estimate Quantiles for Guiding Physical Sampling

Isabel M. Rayas Fernández[†], Christopher E. Denniston[†], David A. Caron, Gaurav S. Sukhatme[‡]

Abstract—Scientists interested in studying natural phenomena often take physical samples for later analysis at locations specified by expert heuristics. Instead, we propose to guide scientists’ physical sampling by using a robot to perform an adaptive sampling survey to find locations to suggest that correspond to the quantile values of pre-specified quantiles of interest. We develop a robot planner using novel objective functions to improve the estimates of the quantile values over time and an approach to find locations which correspond to the quantile values. We demonstrate our approach on two different sampling tasks in simulation using previously collected aquatic data and validate it in a field trial. Our approach outperforms objectives that maximize spatial coverage or find extrema in planning and is able to localize the quantile spatial locations.

I. INTRODUCTION

In order to understand biological phenomena, scientists take physical samples for analyses, often in concert with precision instruments, at specific locations to characterize the biological community and the contextual environmental conditions at the site. For example, marine biologists may be interested in using the concentration of chlorophyll present in a body of water to guide physical sampling of algal blooms, or agricultural scientists may be interested in using crop health to guide physical sampling of plants. Scientists later analyze these physical samples in a laboratory setting, which may be an expensive process. Traditionally, expert heuristics underpin the selection of physical sampling locations. In contrast, we propose performing an adaptive robotic survey to find locations of interest for physical sampling. To specify these locations, we propose quantiling the distribution of interest so that the scientists can take physical samples at the quantiles they are interested in. For instance, if a marine biologist is interested in taking 9 physical water samples that are spread over a range of chlorophyll concentrations, they may choose to sample the deciles of the concentration. If only a small number of physical samples can be taken and the upper extrema values are of interest, they may choose to take samples at the (0.90, 0.95, 0.99) quantiles. Our goal is to guide physical sampling for scientists by using a robot

[†] Equal contribution. {rayas, cdennist}@usc.edu
All authors are with the University of Southern California.

[‡] G.S. Sukhatme holds concurrent appointments as a Professor at USC and as an Amazon Scholar. This paper describes work performed at USC and is not associated with Amazon.

This work was supported in part by the Southern California Coastal Water Research Project Authority under prime funding from the California State Water Resources Control Board on agreement number 19-003-150 and in part by USDA/NIFA award 2017-67007-26154.

This material is based upon work supported by the National Science Foundation Graduate Research Fellowship Program under Grant No. DGE-1842487. Any opinions, findings, and conclusions or recommendations expressed in this material are those of the author(s) and do not necessarily reflect the views of the National Science Foundation.

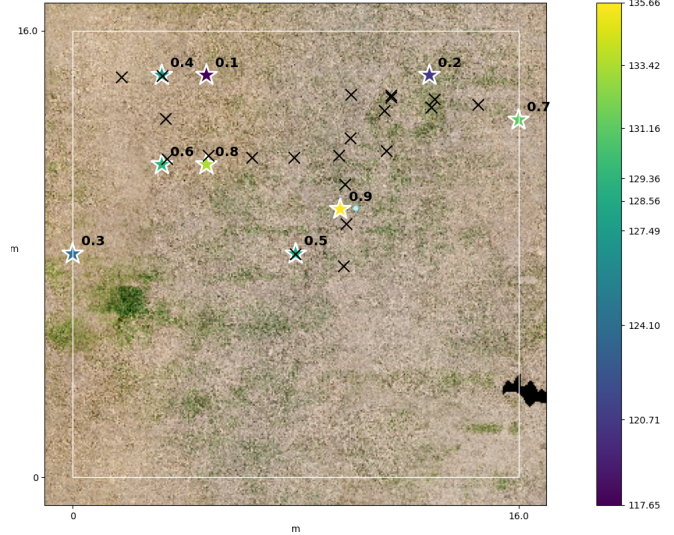


Fig. 1: Visualization of a field trial modeling a crop health task. Crosses are locations where a drone took images. The 9 stars show locations suggested by the drone to sample for the deciles. Darker stars correspond to higher quantiles. The measurement of interest is the amount of green in each pixel. The experiment was geofenced within the white border.

to perform an adaptive survey and then finding locations to suggest based on the measurements it takes. Specifically, we aim to find the desired quantile values of the measurement distribution by adaptively selecting robot measurement locations to maximize an objective function, and produce suggested locations for physical sampling that are likely to contain the estimated quantile values. We develop our method using an adaptive sampling formulation¹ and show that it outperforms an entropy- or Bayesian optimization-based objective baseline. Our contributions are:

- A planner with custom objective functions for adaptively increasing the quality of estimated quantiles;
- A method to select spatial locations which have the values estimated for the quantiles;
- Quantitative evaluation of our method on point and camera sensors with previously collected aquatic datasets;
- A demonstration of our method on a robot in a real-world crop health estimation task.

II. RELATED WORK

Adaptive sampling has a long history in use for studying biological phenomena [1], [2]. Often, the objective in adap-

¹We use adaptive sampling to mean an algorithm by which a robot adaptively takes measurements of a value, and physical sampling to refer to a scientist gathering matter from the environment to analyze later.

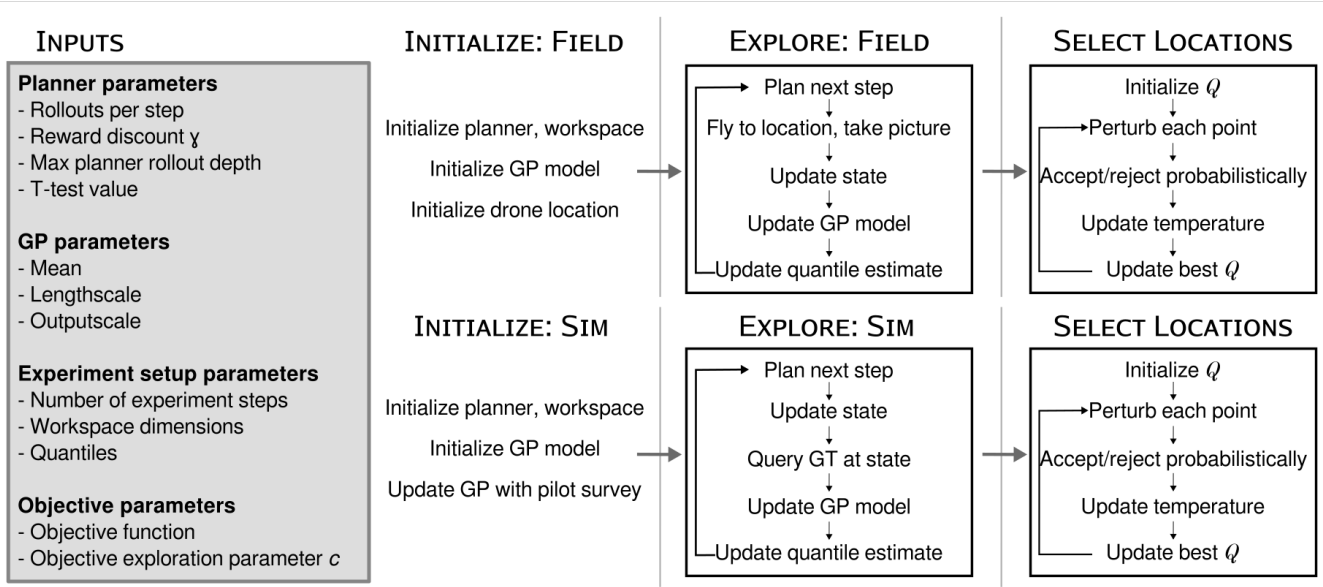


Fig. 2: **Full system.** The first phase is initialization. The middle phase is exploration where the robot plans motions, takes measurements, and updates its model of the distribution and quantile estimates. The final phase of selecting suggested locations (illustrated here by simulated annealing optimization) to represent estimated quantile values can be done offline.

tive sampling is to generate good coverage of a distributed phenomenon using an information theoretic objective such as entropy [3] or mutual information [4]. Other common objectives include finding the highest concentration location [5] or sampling near hotspots [6]. Adaptive sampling has also been used in an objective for surgical robots with the goal of discovering tumors [7]. These specialized objective functions are typically tuned to locate a single specific point, often the extrema, by increasing the quality of the estimate of the underlying concentration. Selecting physical sampling locations using adaptive surveys have typically focused on finding high-concentration areas from which to sample and perform the sampling onboard the robot [8].

Planning for adaptive sampling as a partially observable Markov decision process (POMDP) has been explored [9]; previous works have used this for finding maxima [5] and to adapt the parameters of a rollout-based POMDP solver online to improve its efficiency for adaptive sampling [2].

Bayesian optimization objectives are used to locate extreme values or areas of high concentration and have shown success in doing so in simulation and in real field scenarios [5], [10], [11]. Previous works have also investigated directly calculating the quantile values for distributions at points using specialized loss functions to extend the notion of uncertainty in Gaussian processes, but these do not directly transfer to our setting because they only estimate the quantiles of a specific location [12], [13].

III. BACKGROUND

Gaussian Processes (GPs) are non-parametric models with uncertainty quantification which are widely used for adaptive sampling. They approximate an unknown function from its known outputs by computing the similarity between points from a kernel function [14]. GPs have been used to

represent the belief distribution from observations in POMDP formulations of Bayesian optimization and informed path planning [9], [5], [2]. A GP can be used to estimate the value $\mu(x)$ and variance $\sigma^2(x)$ at a specific location x .

Online Adaptive Sampling consists of alternating between planning and taking an action, which usually corresponds to moving and measuring a value at the new location. A plan described by a partial trajectory p is created to maximize some objective function f over the measured locations X and measured values Y . The combined plan P is the concatenation of partial trajectories p . The plan and act steps are iterated until the cost $c(P)$ exceeds some predefined budget. Formally, this is described by $P^* = \operatorname{argmax}_{P \in \Phi} f(P) | c(P) \leq B$ where Φ is the space of full trajectories, and P^* is the optimal trajectory [15], [2].

Adaptive Sampling as a Partially Observable Markov Decision Process (POMDP) provides a formulation for planning for taking measurements. POMDPs are a framework that can determine optimal actions when the environment is not fully observable or there is uncertainty in the environment. Using observations as measurements from the environment and a GP to represent the belief distribution, Bayesian optimization can be formulated as a Bayesian search game [9]. Measurements from the environment $GT(x)$ constitute observations which are partially observable components of the overall environment GT . To adapt the Bayesian search game formulation to adaptive sampling, the belief state is augmented with the state of the robot x and the actions the planner is allowed to take are restricted to local movements which are feasible for the robot [5]. A complete description of the POMDP for adaptive sampling can be seen in table I.

Estimation of Quantiles and Quantile Standard Error has been proposed using statistical techniques. We estimate

POMDP	Adaptive Sampling
States	Robot position g_t , Underlying unknown function GT
Actions	Neighboring search points g_{t+1}
Observations	Robot position g_t , Measured location(s) $x_t = o(g_t)$ Measured value(s) $y_t = GT(x_t)$
Belief	$GP(y_{1:t} g_{1:t})$
Rewards	$f(x_t)$

TABLE I: **Adaptive Sampling as a POMDP.** After [9], [2].

the quantile value from measurements using $\tilde{v} = x_{\lfloor h \rfloor} + (h - \lfloor h \rfloor)(x_{\lceil h \rceil} - x_{\lfloor h \rfloor})$ where $h = (n - 1)q + 1$, n is the number of measurements, and q is the quantile (Equation 7 in [16])². Given a probability density function p , the standard error of the q th quantile is $\frac{\sqrt{q(1-q)}}{\sqrt{np(\tilde{v})}}$. This method requires p , which is typically not known. To estimate p from samples, a density estimate can be constructed [17]. Here we use a Gaussian Kernel density estimator. Another method to estimate the confidence interval is the Maritz-Jarrett method [18]. The standard error for quantile estimates may also be estimated through bootstrap or jackknife methods which involve calculating the quantiles over repeatedly sampled subsets of the data. These methods can be slow for large datasets and require many iterations to converge.

Continuous Non-Convex Gradient-Free Optimization is used to solve general black-box optimization problems. One common approach is the cross-entropy (CE) method [19]. CE works by maintaining an estimate about the distribution of good solutions, and iteratively updating the distribution parameters based on the quality of the solutions sampled at each step, where the quality is determined via some function of the solution configuration. More precisely, a prior Pr and a posterior Po set of samples are maintained. Po contains n configurations sampled from a Gaussian distribution defined by parameters $\tilde{\mu}$ and $\tilde{\sigma}$. $\tilde{\mu}$ and $\tilde{\sigma}$ are computed from Pr , which is the best $\eta\%$ configurations from Po . This continues iteratively for a fixed number of iterations or until a stopping criterion is met. By taking these iterative steps, CE minimizes the cross-entropy between the maintained distribution and a target distribution [19].

Another popular optimization method is simulated annealing (SA) [20], an iterative improvement algorithm inspired by statistical mechanics. SA optimizes an energy function similar to a loss function in other optimization schemes, as configurations with lower energy are preferred. SA begins with a temperature $T = T_{\max}$. At each iteration, T is decreased exponentially, and the configuration is slightly perturbed randomly. The perturbed state is either accepted or rejected probabilistically based on its energy and T . The algorithm terminates when T reaches a given threshold.

IV. FORMULATION

We use a grid-based representation of the planning space, \mathbf{G}^* , which defines the set of locations that the robot could visit. For a robot that moves in \mathbb{R}^d , $\mathbf{G}^* \subset \mathbb{R}^d$ and $|\mathbf{G}^*| < \infty$. \mathbf{X}^* is the set of locations the robot could measure. If the robot sensor has finer resolution than \mathbf{G}^* , then $|\mathbf{X}^*| > |\mathbf{G}^*|$. We define \mathbf{X} as the locations the robot has already

measured and \mathbf{Y}^* and \mathbf{Y} as the values at all possible measured locations, and the values the robot has measured, respectively.

We define the ground truth quantile values as $V = \text{quantiles}(\mathbf{Y}^*, Q)$, where *quantiles* is a function which computes the quantiles Q of a set of values. To define the robot's estimated quantile values, we compute $\tilde{V} = \text{quantiles}(\mu(\mathbf{X}^*), Q)$, that is, the quantile values of the predicted values from the robot's current GP for all locations the robot could sense. This is done to prevent the number of measurements from which the quantile values are estimated from changing as the robot explores (instead of, e.g. using $\mu(\mathbf{X})$). To assess estimation accuracy, we compute the error using $l_p(\tilde{V}, V)$ where l_p is an accuracy estimate. During planning, we aim to minimize this error by taking actions which maximize an objective function f .

To suggest locations for the quantile values, we aim to find a set of $|Q|$ locations \mathcal{Q} in the continuous space whose values at those locations are equal to the quantile ground-truth values. A set of locations is defined as $\mathcal{Q} \in \mathcal{Q}^*$ where $\mathcal{Q}^* \subset \mathbb{R}^{d \times |Q|}$ and \mathcal{Q}^* is continuous over the space of \mathbf{G}^* . In practice, the robot only has knowledge of \tilde{V} during the selection process, so the problem of finding $\tilde{\mathcal{Q}}$ can be stated as shown in eq. (1) with some selection loss function l_s .

$$\begin{aligned} \mathcal{Q}[i] = x \in \mathbb{R}^d \quad \text{s.t.} \quad & GT(\mathcal{Q}[i]) = V[i] \quad \forall i \in [1, |Q|] \\ \tilde{\mathcal{Q}} = \arg \min_{\mathcal{Q}' \subset \mathcal{Q}^*} & l_s(\tilde{V}, \mathcal{Q}') \end{aligned} \quad (1)$$

V. APPROACH

Figure 2 illustrates our method. To plan which locations to sample, the robot uses the POMDP formulation of adaptive sampling. In order to generate a policy, we use the partially observable Monte Carlo planner (POMCP) [21]. POMCP uses Monte Carlo tree search to create a policy tree. To expand the tree and estimate rewards, the tree is traversed until a leaf node is reached. Typically, from the leaf node, a random policy is executed until the discounted reward is smaller than some value ϵ . We modify the rollout reward to be fixed horizon which gives a reward of zero once a certain depth is reached. We adopt the t-test heuristic for taking multiple steps from a POMCP plan for adaptive sampling to improve performance of the planner with fewer rollouts [2]. Because the observations $GT(x)$ for unseen locations are not known during planning, the predicted value from the GP conditioned on the previous observations is used [5].

A. Planning Objective Functions

Entropy is a common objective function for adaptive sampling when only good spatial coverage of the environment is desired [3], [4], [22]. It provides a good baseline as it is often used when the specific values of the underlying concentration are unknown. Entropy is defined by rescaling the variance in the GP at the location according to eq. (2):

$$f_{\text{en}}(x_i) = \frac{1}{2} \log(2\pi e \sigma^2(x_i)) \quad (2)$$

²This is the default in the `numpy` Python package

Another objective function we compare against is expected improvement, which is widely used in Bayesian optimization for finding maxima [23], [24]. Expected improvement favors actions that offer the best improvement over the current maximal value, with an added exploration term ξ to encourage diverse exploration. The expected improvement objective function is defined according to eq. (3):

$$I = (\mu(x_i) - \max(\mu(\mathbf{X}^*)) - \xi) \quad Z = \frac{I}{\sigma^2(x_i)}$$

$$f_{ei}(x_i) = \begin{cases} 0 & \sigma^2(x_i) = 0 \\ I\Phi(Z) + \sigma(x)\phi(Z) & \sigma^2(x_i) > 0 \end{cases} \quad (3)$$

where Φ and ϕ are the CDF and PDF of the normal distribution.

We develop two novel objective functions to improve the quality of planning for estimating quantile values. Both functions compare a measure of the quality of the quantiles estimated by the GP before and after adding the measurement to the GP. For both functions, we include an exploration term $c\sigma^2(x_i)$, inspired by the upper confidence bound acquisition function [5], where c is a chosen constant. For both objective functions, $A = GP(\mathbf{X}_{0:i-1}, \mathbf{Y}_{0:i-1}; \theta)$ is a GP conditioned on the points before measuring a proposed value, and $B = GP(\mathbf{X}_{0:i-1} \cup \{x_i\}, \mathbf{Y}_{0:i-1} \cup \{y_i\}; \theta)$ is a GP conditioned on the previous and proposed measurements, where θ are GP parameters. For both proposed objective functions we use eq. (4):

$$f(x_i) = \frac{\delta}{|Q|} + c\sigma^2(x_i) \quad (4)$$

where δ is defined by the objective.

The first objective function, which we call *quantile change*, is based on the idea of seeking out values which change the estimate of the quantile values by directly comparing the estimated quantiles before and after adding the measured values to the GP. The idea behind this is that a measurement which changes the estimate of the quantiles indicates that the quantiles are over- or under-estimated. This can be seen in in eq. (5):

$$\delta_{qc} = \|\text{quantile}(\mu_A(\mathbf{X}^*), Q) - \text{quantile}(\mu_B(\mathbf{X}^*), Q)\|_1 \quad (5)$$

The second objective function we develop, which we call *quantile standard error*, is based on the change in the estimate of the standard error for the estimated quantiles. It draws from the same idea that if the uncertainty in the quantile estimate changes after observing a measured value, then it will change the estimate of the quantile values, shown in eq. (6):

$$\delta_{se} = \|\text{se}(\mu_A(\mathbf{X}^*), Q) - \text{se}(\mu_B(\mathbf{X}^*), Q)\|_1 \quad (6)$$

se is an estimate of the standard error of the quantile estimate for quantiles Q . se uses a Gaussian kernel density estimate (we found it faster and more stable than the Maritz-Jarrett estimator, and considerably faster than sampling based estimators, such as bootstrap and jackknife). To compute the

objective function over a set of measured points, we average the objective function at each point.

B. Finding Optimal Locations

Our final goal is to produce a set of $|Q|$ locations Q , at which the concentration values will be equal to V , the values of the quantiles Q . The problem of finding locations that represent Q is difficult because the objective function over arbitrary phenomena in natural environments will likely be non-convex, and in a real-world deployment, the robot will only have an estimate \hat{V} of the V it is searching for.

With the location selection problem formulation as in eq. 1, we use $l_s(\hat{V}, \hat{Q}) = \|\hat{V} - \mu(\hat{Q})\|_2$. The selection process can be done offline, since it does not affect planning. The optimizer runs using \hat{V} and returns the suggested sampling locations \hat{Q} . We use both simulated annealing (SA) and cross-entropy (CE) optimization methods in our experiments.

VI. EXPERIMENTS

To evaluate our approach, we compare against baselines in two different adaptive sampling tasks in simulation using datasets collected in the real world.

In the first task, a drone is simulated with a virtual camera over orthomosaics collected of a lake using a hyperspectral sensor. The drone collects many measurements from one location with each point being a pixel in a downsampled image. As a proxy for chlorophyll concentration, we are interested in quantiling the pixel intensity. The drone maintains a constant altitude and moves in a 2D plane with a north-fixed yaw and makes a move in either the x or y direction per step. The two orthomosaics, A and B, are taken in the same location but on different days and times.

In the second task, an autonomous underwater vehicle (AUV) is tasked with exploring a 3D workspace interpolated from a 3D lawnmower survey collected previously. The lawnmower survey is interpolated using a GP to the planning grid. At each step the AUV may move in one x , y , or z direction. The AUV takes five evenly spaced samples when moving between locations. The two AUV surveys, C and D, are taken in the same reservoir at different times and in different areas of the lake.

A. Quantile Estimate Improvement

To compare the ability of our proposed objective functions, quantile change (eq. (5)) and quantile standard error (eq. (6)), we compare against a baseline entropy objective function (eq. (2)). For each task, we compare on two different datasets (A/B, C/D) and three different quantiles: deciles (0.1, 0.2, . . . 0.8, 0.9), quartiles (0.25, 0.5, 0.75) and upper extrema (0.9, 0.95, 0.99). For the upper extrema quantiles, we also compare against expected improvement (eq. (3)), as it is similar to a Bayesian optimization based adaptive sampling task. In the planner, we use $\gamma = 0.9$, $t\text{-test_value} = 0.1$, and each trial is run over 3 seeds. The objective c parameter is set to the approximate magnitude of the rewards seen for each environment, which we found experimentally to be an adequate value. The parameters for the GPs were all found experimentally.

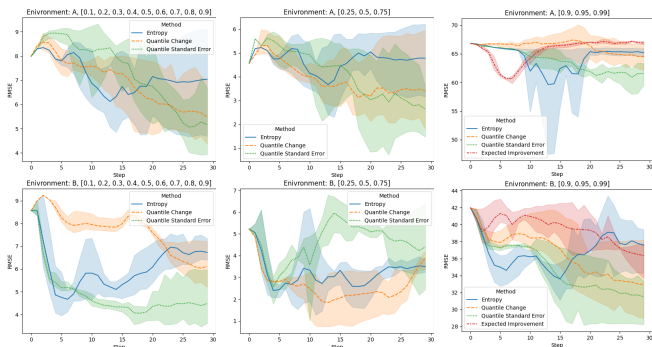


Fig. 3: **Simulated drone experiments with real data.** Error between ground truth quantile values and estimated quantile values in a task with a simulated drone with a camera using data collected in Clearlake, California.

1) *Drone with Camera:* For this task, the drone is allowed to take 30 simulated pictures out of a grid with about 300 positions. Each simulated picture is downsampled to 8 by 5 pixels with 37.1° by 27.6° field of view, similar to the drone used in the field trial reported in section VI-C. For each trial, the GP used by the robot is seeded with 100 evenly spaced points across the workspace. In the planner, 300 rollouts per step are used and the max planning depth is 7.

Figure 3 shows the results of planning with the proposed objective functions. Quantile change and quantile standard error outperform the baseline entropy in estimating the deciles and upper extrema. In quartiles in environment A, both proposed methods perform well, but in environment B entropy outperforms our methods. We believe this because this specific configuration is the most difficult task as each method performs worse at the end than they do at 5 steps. For the extrema, both methods perform better than expected improvement and entropy outperforms expected improvement in environment A. We believe this is because expected improvement only looks to improve the maximal value and does not do a good job localizing high concentration areas instead of a single point.

2) *AUV with Chlorophyll Sensor:* The AUV is simulated for 200 steps in a $12 \times 14 \times 2$ grid. The planner uses 130 rollouts per step and a max depth of 10. The GP is seeded with values from 50 locations.

Figure 4 shows the results of this experiment. Quantile standard error outperforms entropy in environment C when estimating deciles and quartiles, and performs equally well as entropy in all other tasks besides estimating the extrema in environment D. Quantile change performs poorly in most tasks, and expected improvement performs poorly in estimating the extrema due to similar issues as the previous task.

B. Physical Location Selection

To produce suggested physical sampling locations, we use the optimization algorithms simulated annealing (SA) and cross-entropy (CE) with the results from the quantile estimation task.

For SA, we use $T_{\max} = 1000$, $T_{\min} = 1$, and cooling rate $cr = 0.01$ which leads to approximately 690 optimization steps. For CE, we use $\alpha = 0.9$, $\eta = 0.9$, $n_{\text{samples}} = 50$,

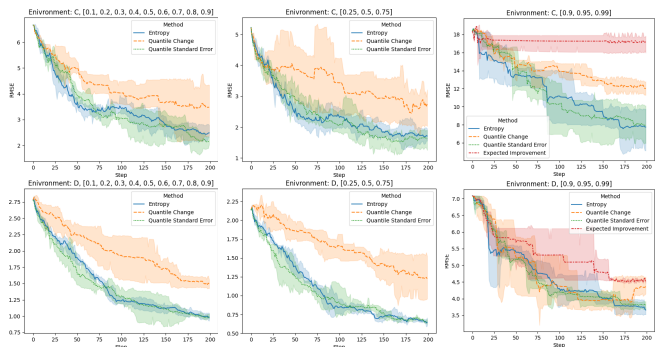


Fig. 4: **Simulated AUV experiments with real data.** Error between ground truth quantile values and estimated quantile values. Dataset collected from a reservoir in California.

	Simulated Annealing (SA)		Cross Entropy (CE)	
	Estimated	GT	Estimated	GT
Drone				
deciles	0.06 ± 0.05	14.76 ± 5.96	0.73 ± 0.73	14.34 ± 2.88
quartiles	0.04 ± 0.09	10.51 ± 3.42	0.04 ± 0.03	11.56 ± 3.55
extrema	0.10 ± 0.04	64.15 ± 18.30	1.59 ± 0.91	59.00 ± 14.22
AUV				
deciles	0.02 ± 0.02	10.55 ± 7.23	0.67 ± 0.50	12.25 ± 9.00
quartiles	0.01 ± 0.01	8.02 ± 7.74	0.05 ± 0.03	8.75 ± 7.26
extrema	0.39 ± 0.41	23.23 ± 15.67	3.70 ± 3.50	22.97 ± 16.04

TABLE II: **Final optimizer loss for experiments in simulation.** *Estimated* columns: loss at selected locations $\|(\tilde{V} - \mu(\tilde{Q}))\|_2$; *GT* columns $\|(V - GT(\tilde{Q}))\|_2$. Results averaged over the 2 environments and 3 random seeds. Units are pixel brightness for Drone and $\mu g/L$ chlorophyll for AUV.

and $n_{\text{iterations}} = 100$ where α is a weighting factor on new samples, n_{samples} is the number of different Q_s that are kept in the posterior, and $n_{\text{iterations}}$ is the number of optimization steps. We found experimentally that for higher n_{samples} or $n_{\text{iterations}}$, CE becomes very computationally intensive without producing better output. Overall, we found that SA tended to be faster and produce slightly better solutions, but in general both methods perform similarly for most experiments in terms of $l_s(\tilde{V}, \tilde{Q})$.

1) *Drone with Camera:* Figure 5 shows results for one seed of the drone with a camera sensor when monitoring deciles. Although the suggested locations, shown as white stars, differ spatially in all 4 versions, they generally align quite closely with the quantile value estimates \tilde{V} , shown by the contours. This demonstrates the ability of the optimizers to produce good suggestions to guide physical sampling, given that the robot has had a chance to explore the environment sufficiently.

The bottom part of figure 5 shows the same locations on top of the orthomosaic of what the drone measured during exploration. This part of the figure highlights the difficulty of the problem of adaptive sampling for quantiles. With only partial knowledge of the environment, the robot’s model of the phenomenon will vary based on the particular points it visited, which in turn affects the estimates of the quantiles. Given a set of estimated quantile values, the location selection optimizer consistently produces good suggested locations for those estimates.

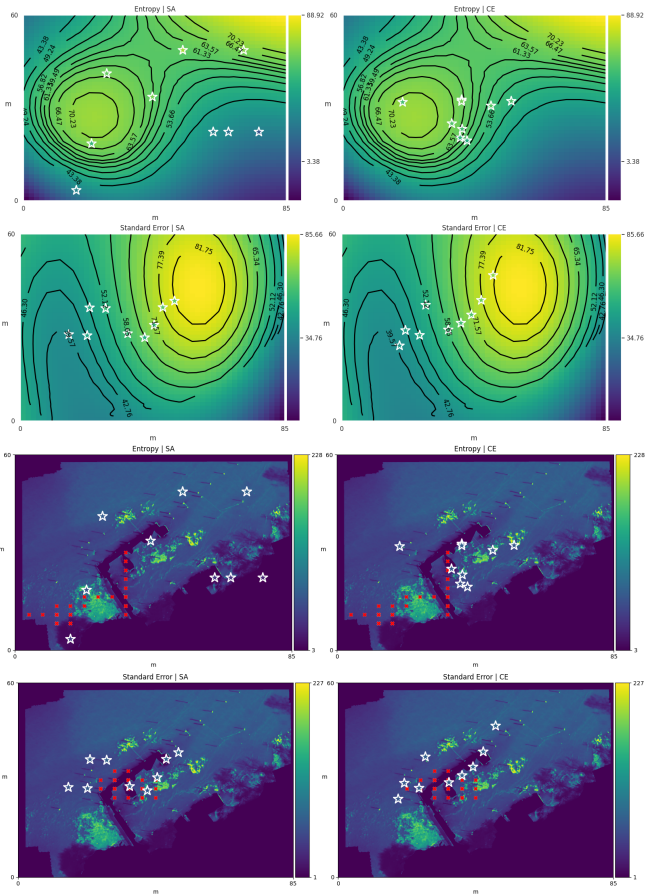


Fig. 5: Physical locations (white stars) selected by the optimizers SA (left) and CE (right) for deciles. Entropy and quantile standard error are the planning objective functions in the 1st/3rd and 2nd/4th rows, respectively. [Top] Black lines: model prediction contours. [Bottom] Red crosses: locations the robot visited, overlaid on the ground truth raster image.

2) *AUV with Chlorophyll Sensor*: For the AUV, figure 6 shows the suggested locations for the quartiles for one seed. Similar to the experiment with the drone, the suggested locations correspond well to \tilde{V} produced by the planner.

Table II shows final loss scores of the optimizers in both the Drone and the AUV experiments for the selected locations using the robot model loss $\|\tilde{V} - \mu(\tilde{Q})\|_2$ and the ground truth model loss $\|(V - GT(\tilde{Q}))\|_2$. The robot model loss is consistently near 0 with the exception of CE when estimating the extrema, which is slightly higher for both the Drone and AUV environments. This shows that the optimizer consistently finds near-optimal locations to represent \tilde{V} . In contrast, the ground truth model loss is higher, illustrating that the optimizer only has knowledge of the estimated quantile values. Quartiles appear to be the most well-represented in terms of the ground truth loss, which corresponds to the lower error seen in fig. 3 and fig. 4.

C. Field trial

In our final experiment we demonstrate our method on a crop health monitoring task, where the objective is to estimate the deciles of the green present in each pixel of the

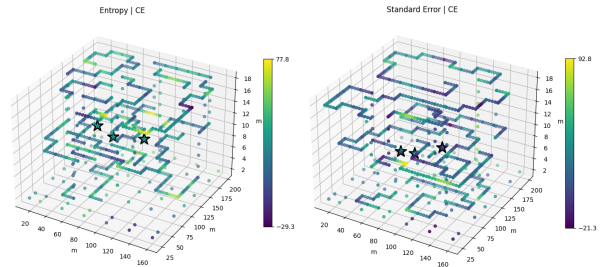


Fig. 6: Physical locations (stars) selected by the CE optimizer for the quartiles with an AUV using a chlorophyll point sensor. Entropy (left) and quantile standard error (right) are the planning objective functions. Blue/green points are the measured locations X .

images (we use green as a proxy for plant health). We use a commercial, off-the-shelf drone with a standard camera to take measurements of the field at a constant height of 3m. Similar to the simulated drone, the drone in this experiment moves in a 2D plane with a north-fixed yaw. The drone can take 20 pictures (planning steps) in a 16×16 m square grid, where $|G^*| = 10 \times 10 = 100$ points, and each picture is downsampled to 8 by 5 pixels. For planning, we use the quantile change objective function because it performs well for camera sensors and is faster than quantile standard error. Figure 1 shows the resulting suggested locations using SA based on the 20 steps shown that the robot took.

VII. CONCLUSION

Scientists traditionally take physical samples at locations selected using heuristics. They later analyze these samples in a laboratory to characterize a phenomenon of interest (e.g., the distribution of algae in the water). We propose to, instead, choose these physical sampling sites by first performing an adaptive sampling survey with a robot and then proposing locations which correspond to the quantiles of the distribution. To accomplish this, we propose two novel objective functions, quantile change and quantile standard error, for improving the estimates of quantile values through adaptive sampling. We test these in three settings: a drone with a camera sensor over lake imagery, an underwater vehicle taking chlorophyll measurements, and a field trial using a drone for a crop health monitoring task. Our objective functions perform well on these tasks and specifically outperform information theoretic and Bayesian optimization baselines. We also show that optimization methods like simulated annealing and cross-entropy can produce physical locations in the environment representative of a set of quantiles of interest when combined with an adaptive survey for those quantiles. Our approach can be used to guide physical sampling in real field scenarios, as demonstrated by our field trial. Experimentally finding parameters was difficult for both the baselines and our proposed methodology, particularly for the GP; this is a direction for future work. We also plan to incorporate our physical sampling suggestions into a larger field campaign involving multiple scientists.

REFERENCES

- [1] T. O. Fossum, J. Eidsvik, I. Ellingsen, M. O. Alver, G. M. Fragoso, G. Johnsen, R. Mendes, M. Ludvigsen, and K. Rajan, "Information-Driven Robotic Sampling in the Coastal Ocean," *Journal of Field Robotics*, vol. 35, no. 7, pp. 1101–1121, 2018. [Online]. Available: <https://onlinelibrary.wiley.com/doi/abs/10.1002/rob.21805>
- [2] C. E. Denniston, G. Salhotra, D. A. Caron, and G. S. Sukhatme, "Adaptive Sampling using POMDPs with Domain-Specific Considerations," in *2020 International Conference on Robotics and Automation*, Oct 2020. [Online]. Available: <http://robotics.usc.edu/publications/1115/>
- [3] S. Kemna, O. Kroemer, and G. S. Sukhatme, "Pilot Surveys for Adaptive Informative Sampling," in *2018 IEEE International Conference on Robotics and Automation (ICRA)*, May 2018, pp. 6417–6424, iSSN: 2577-087X.
- [4] C. Guestrin, A. Krause, and A. P. Singh, "Near-optimal sensor placements in Gaussian processes," in *Proceedings of the 22nd international conference on Machine learning - ICML '05*. Bonn, Germany: ACM Press, 2005, pp. 265–272.
- [5] R. Marchant, F. Ramos, and S. Sanner, "Sequential Bayesian optimization for spatial-temporal monitoring," in *Proceedings of the Thirtieth Conference on Uncertainty in Artificial Intelligence*, ser. UAI'14. Arlington, Virginia, USA: AUAI Press, Jul. 2014, pp. 553–562.
- [6] S. McCammon and G. A. Hollinger, "Topological Hotspot Identification for Informative Path Planning with a Marine Robot," in *2018 IEEE International Conference on Robotics and Automation (ICRA)*. IEEE, May 2018, pp. 1–9.
- [7] H. Salman, E. Ayvali, R. A. Srivatsan, Y. Ma, N. Zevallos, R. Yasin, L. Wang, N. Simaan, and H. Choset, "Trajectory-optimized sensing for active search of tissue abnormalities in robotic surgery," in *2018 IEEE International Conference on Robotics and Automation (ICRA)*, 2018, pp. 5356–5363.
- [8] J. Das, F. Py, J. B. Harvey, J. P. Ryan, A. Gellene, R. Graham, D. A. Caron, K. Rajan, and G. S. Sukhatme, "Data-driven robotic sampling for marine ecosystem monitoring," *The International Journal of Robotics Research*, vol. 34, no. 12, pp. 1435–1452, Oct. 2015, publisher: SAGE PublicationsSage UK: London, England.
- [9] M. Toussaint, "The Bayesian Search Game," in *Theory and Principled Methods for the Design of Metaheuristics*, Y. Borenstein and A. Moraglio, Eds. Berlin, Heidelberg: Springer Berlin Heidelberg, 2014, pp. 129–144, series Title: Natural Computing Series.
- [10] A. Blanchard and T. Sapsis, "Informative Path Planning for Extreme Anomaly Detection in Environment Exploration and Monitoring," *arXiv:2005.10040 [cs, stat]*, Apr. 2021, arXiv: 2005.10040.
- [11] J. R. Souza, R. Marchant, L. Ott, D. F. Wolf, and F. Ramos, "Bayesian optimisation for active perception and smooth navigation," in *2014 IEEE International Conference on Robotics and Automation (ICRA)*, May 2014, pp. 4081–4087, iSSN: 1050-4729.
- [12] A. Boukouvalas, R. Barillec, and D. Cornford, "Direct Gaussian Process Quantile Regression Using Expectation Propagation," in *Proceedings of the 29th International Conference on International Conference on Machine Learning*, ser. ICML'12. Madison, WI, USA: Omnipress, 2012, p. 939–946.
- [13] B. J. Reich, "Spatiotemporal quantile regression for detecting distributional changes in environmental processes," *Journal of the Royal Statistical Society: Series C (Applied Statistics)*, vol. 61, no. 4, pp. 535–553, 2012, eprint: <https://rss.onlinelibrary.wiley.com/doi/pdf/10.1111/j.1467-9876.2011.01025.x>.
- [14] C. E. Rasmussen and C. K. I. Williams, *Gaussian Processes for Machine Learning*. MIT press, 2006, iSSN: 0129-0657.
- [15] G. A. Hollinger and G. S. Sukhatme, "Sampling-based robotic information gathering algorithms," *The International Journal of Robotics Research*, vol. 33, no. 9, pp. 1271–1287, 2014.
- [16] R. J. Hyndman and Y. Fan, "Sample Quantiles in Statistical Packages," *The American Statistician*, vol. 50, no. 4, pp. 361–365, 1996, publisher: [American Statistical Association, Taylor & Francis, Ltd.].
- [17] R. Wilcox, *Introduction to Robust Estimation and Hypothesis Testing (Third Edition)*, 3rd ed., ser. Statistical Modeling and Decision Science. Boston: Academic Press, 2012.
- [18] J. S. Maritz and R. G. Jarrett, "A Note on Estimating the Variance of the Sample Median," *Journal of the American Statistical Association*, vol. 73, no. 361, pp. 194–196, Mar. 1978, publisher: Taylor & Francis eprint: <https://www.tandfonline.com/doi/pdf/10.1080/01621459.1978.10480027>.
- [19] P.-T. De Boer, D. P. Kroese, S. Mannor, and R. Y. Rubinstein, "A tutorial on the cross-entropy method," *Annals of operations research*, vol. 134, no. 1, pp. 19–67, 2005.
- [20] S. Kirkpatrick, C. D. Gelatt Jr, and M. P. Vecchi, "Optimization by Simulated Annealing," in *Readings in Computer Vision*. Elsevier, 1987, pp. 606–615.
- [21] D. Silver and J. Veness, "Monte-Carlo Planning in Large POMDPs," in *Advances in Neural Information Processing Systems*, J. Lafferty, C. Williams, J. Shawe-Taylor, R. Zemel, and A. Culotta, Eds., vol. 23. Curran Associates, Inc., 2010.
- [22] C. Denniston, A. Kumaraguru, and G. S. Sukhatme, "Comparison of Path Planning Approaches for Harmful Algal Bloom Monitoring," in *OCEANS 2019 MTS/IEEE SEATTLE*, Oct. 2019, pp. 1–9, iSSN: 0197-7385.
- [23] D. R. Jones, M. Schonlau, and W. J. Welch, "Efficient Global Optimization of Expensive Black-Box Functions," *Journal of Global Optimization*, vol. 13, no. 4, pp. 455–492, Dec. 1998.
- [24] C. Qin, D. Klabjan, and D. Russo, "Improving the expected improvement algorithm," in *Proceedings of the 31st International Conference on Neural Information Processing Systems*, ser. NIPS'17. Red Hook, NY, USA: Curran Associates Inc., 2017, p. 5387–5397.